

## Ballasted Track on Vibrating Bridge Decks: Physical Mechanisms, Empirical Findings, and a Proposal for Assessment

Matthias Baeßler \* and Patrick Simon 

*Bundesanstalt für Materialforschung und -prüfung  
Unter den Eichen 87, 12205 Berlin, Germany  
\*matthias.baessler@bam.de*

Received 7 December 2024

Accepted 5 February 2025

Published 29 April 2025

This paper summarizes the key findings and physical mechanisms and provides information on open questions and the assessment of railway bridge superstructure vibrations. Bridges are classic disruption points on a railway track. If bridge superstructures are dynamically excited by train traffic, the vertical accelerations of the track must be considered. For a ballasted track, this can lead to the destabilization of the ballast track, as the bridge superstructure acts like a vibrating table. In this respect, the paper explains in more detail what is meant by destabilization, when this destabilization occurs and how various influencing parameters such as acceleration amplitude, the vibration sequence and frequency affect its occurrence. In the InBridge4EU project, gaps in knowledge such as the effect of single impulse loads are being investigated experimentally. A new test facility has been set up for this purpose, the initial results of which are presented here. An essential element in the assessment of this scenario is the stability of the track under high compression forces with simultaneous dynamic excitation of the superstructure. A new approach for the assessment of bridge vibrations with respect to lateral stability is presented.

**Keywords:** Railway bridge dynamics; bridge deck acceleration; ballast destabilization; lateral track stability; track buckling.

### 1. Introduction

Railway bridges perform the task of the substructure as the basis of a railway track in rail transport. It is therefore not surprising that the requirements of the

\*Corresponding author.

This is an Open Access article published by World Scientific Publishing Company. It is distributed under the terms of the Creative Commons Attribution 4.0 (CC BY) License, which permits use, distribution and reproduction in any medium, provided the original work is properly cited.

vehicle, the track and their interaction have a decisive influence on the design of the bridge structure. The service limit states can be decisive for the design of the railway bridges, being in fact ultimate limit states (ULS) with respect to the safety of the traffic.<sup>1</sup> Deflections of the superstructure when a train passes over it can lead to unpleasant accelerations for the passenger. For reasons of traveling comfort, the superstructure deflections, depending on speed and bridge length, have been limited to small amplitudes. A side effect of the very small permissible values is that the vibration response of the bridge structure usually remains small. However, for unfavorable vehicle-track combinations, this can lead to structural resonances for certain traveling speeds.

It is known from the dynamic calculations by the ERRI D214 Committee<sup>2</sup> that, despite compliance with the deflection criterion, vibration amplitudes of the bridge superstructure of up to 1.0 g are possible. In France, with the commissioning of the Paris–Lyon line, resonances occurred on some short bridges as a result of train crossings, which manifested themselves in signs of destabilization on the ballasted track. Visible vibrations of individual ballast stones were observed when trains passed over them. Ballast stones moved on the raised ballast shoulder, which led to a lateral track shift and presumably reduced the transverse resistance to the transverse displacement. Loosening, heavy abrasion, formation of longitudinal height and track alignment errors and even voided sleepers were the consequences. The subsequent measurements confirmed the resonance excitation of the superstructure. Acceleration amplitudes greater than 0.7 g were measured, whereby the destabilization of the ballast bed was significant. Some measured acceleration amplitudes were even higher, reaching 0.9 g.

The occurrence of these phenomena shows that two distinct structures interact with one another: The track and the bridge. This interaction may have unforeseen consequences for either one of the structures.

Very extensive numerical and experimental research activities have been carried out internationally to understand and correctly predict the occurrence of resonance phenomena and dynamic interaction in general. The main focus has been the development of numerical prediction models and an accurate estimate of the dynamic parameters of the bridge and the interacting track superstructure. As a consequence, the recent research focuses on stiffness,<sup>3</sup> damping,<sup>4</sup> coupling<sup>5</sup> and shear<sup>6</sup> effects of ballast in the context of railway bridge dynamics. Moliner *et al.*<sup>7</sup> investigate the influence of vertical flexibility of the bearings and transverse vibration modes. Ferreira *et al.*<sup>8</sup> question the current acceleration limit for bridge superstructures. Deck acceleration values above the limit do not have a direct correspondence with current derailment criteria, and running safety is more conditioned by track quality than by bridge resonance. Another set of experimental data studying the coupling of ballast layer on adjacent bridge decks is presented in Galvín *et al.*<sup>9</sup>

This focus on the effects ballasted track has on the (dynamic) properties of bridges is very useful for addressing many issues related to railway bridge dynamics. However, the limit criterion on acceleration prescribed in the design and reassessment codes, such as EN 1990<sup>10</sup> and ÖNORM B 4008-2,<sup>11</sup> is based on the destabilization of the ballasted track. Ballast destabilization is a rough description of uncontrolled deformations in the ballast bed due to dynamic action. Most critical is when the ballasted track is subject to vertical vibrations while at the same time lateral static loads act on the sleepers which leads to the phenomenon of vibration-induced creep.<sup>12</sup> Recent experimental work on ballasted track focusses on lateral vibrations for questions regarding earthquakes,<sup>13</sup> dynamic lateral resistance,<sup>14</sup> or energy dissipation.<sup>4</sup> A recent review of lateral resistance of sleepers<sup>15</sup> lists earthquakes and vertical train loads as dynamic loads on ballasted tracks. The current state of research leads to the conclusion that research is either focused on the effects ballasted track has on the train and bridge dynamics (see previous paragraph) or on issues of track resistance (this paragraph). However, there is no current research on the effect vertical bridge vibrations have on ballasted tracks subject to lateral loads.

This paper proposes to bridge the gap between these two structures by coming from the track and addressing the effects the bridge has on the track. It proceeds by summarizing the physical mechanisms and giving an overview of past and current experimental findings. This leads to a proposal for the assessment of the stability of the ballasted track on vibrating bridge decks.

This paper is restricted to the destabilization of ballasted tracks directly on vibrating bridge decks. Baeßler *et al.*<sup>16</sup> provide a more general discussion on the degradation of ballasted track at bridges in high-speed lines, also considering specific problems at the transition zone. This work is part of the InBridge4EU Project<sup>17</sup> which aims to enhance and harmonize the standards for evaluating the dynamic performance of European railway bridges to improve interoperability, structural analysis, and cost efficiency.


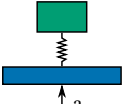
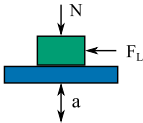
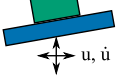
## 2. Vertical Shake Table: From Physical Mechanisms to Scenario-Based Tests on Ballast Track

### 2.1. Introduction

Vertical shake table tests can be best understood based on simple basic mechanical considerations, which are shown in Table 1.

A rigid body that is accelerated with an amplitude opposite to and greater than the gravitational constant during a vibration excitation loses contact with its base from 1 g onwards. This occurs when the table is at the top-most position where it experiences the largest downward acceleration. If the body is elastic or elastically mounted, it is a vibrating system and the increase in vibration transmission when the base is excited can cause the body to completely lose contact force even below an

Table 1. Considerations for a body on a vertical shake table.

	Physical mechanism
	Rigid body on a shake table with harmonic excitation. For $a > 1g$ , the rigid body remains contactless, thereby prone for displacements.
	Rigid body as a mass-spring system on a shake table with harmonic excitation. Due to the transfer function of the mass-spring-system, the critical acceleration amplitude of the table can be below $1g$ .
	Rigid body as a mass-spring system on a shake table with harmonic excitation. The lateral resistance depends on the weight force on the shake table. Intermittently, the lateral resistance gets reduced and can be 0 for $a > 1g$ .
	On an inclined plane, the movement of the body is dependent on the velocity of the movement of the plane in any specific direction.

excitation of  $1g$ . Lateral displacement of the body due to a lateral force is generally counteracted by friction from the weight force. If the weight force of the body is minimized during vibration excitation, the body can be displaced more easily. From these considerations, it becomes clear how the ballast grains connected by contact forces and friction can be displaced more easily or no longer act as a continuum at an excitation close to  $1g$ .

These considerations summarize the first three cases in Table 1. In addition, viscous behavior has been proven theoretically for a body on an inclined plane, where the eventual movement of the sample is dependent on the velocity of the movement of the plane in any specific direction.<sup>18</sup> This pseudo-viscosity can be associated with dynamically excited slopes.

To transfer the basic considerations from a single body on a vibrating table, the complex system of a ballasted superstructure on the bridge must be considered. The ballast track on a bridge is illustrated in Fig. 1. The track on bridges is a continuation of the track on the subgrade. Designs differ in the variants of a boundary by a trough or by an ordinary embankment. Phenomenological observations when this cross-section across the bridge is excited as a vibrating table with high amplitude shows a separation of ballast stones near the surface. However, on an embanked cross-section, lateral movement (flow) can also be observed on the embankment.

## 2.2. Material behavior and loading scenario

The behavior of granular geomaterials such as the ballast fabric under cyclic and dynamic loads has been extensively investigated in the past. Ballast and sand differ



Int. J. Str. Stab. Dyn. Downloaded from www.worldscientific.com  
by 2001:690:2200:9a82:b167:d166:2989:43f8 on 09/08/25. Re-use and distribution is strictly not permitted.

Int. J. Str. Stab. Dyn. Downloaded from www.worldscientific.com  
by 2001:690:2200:9a82:b167:d166:2989:43f8 on 09/08/25. Re-use and distribution is strictly not permitted.

Int. J. Str. Stab. Dyn. Downloaded from www.worldscientific.com  
by 2001:690:2200:9a82:b167:d166:2989:43f8 on 09/08/25. Re-use and distribution is strictly not permitted.

Int. J. Str. Stab. Dyn. Downloaded from www.worldscientific.com  
by 2001:690:2200:9a82:b167:d166:2989:43f8 on 09/08/25. Re-use and distribution is strictly not permitted.

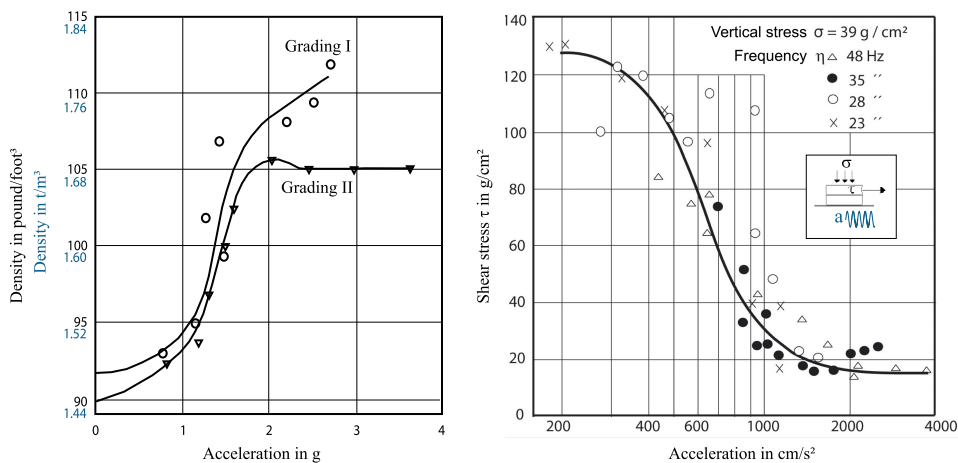


Fig. 2. Compaction achieved on a vibrating table at different acceleration amplitudes according to Gaskin *et al.*<sup>20</sup> (left); Maximum shear stress achieved in the shear test on a shake table at different acceleration amplitudes according to Mogami and Kubo<sup>22</sup> (right).

tests, a close look must be taken at the sample preparation and the complex load application:

(1) **Local picture:** The presented tests with sand and ballast have loose bedding as the initial condition. The granular fabric is compacted by the vibrations of the vibrating table, as visualized in Fig. 3.

On the other hand, a real ballast superstructure is highly compacted before service starts. Dilatant behavior is expected. The scenario for track settlements can be assumed as follows, as Fig. 4 visualizes: (1) ballast is placed and compacted (tamped) on the bridge. Then the bridge-track-system is excited (2) causing a loosening of the ballast fabric (3, dilatancy) and eventually a heave of the sleeper. A reloading of the track due to train passages (4) might lead to small increments of additional settlements (5). The described procedure exemplifies a general

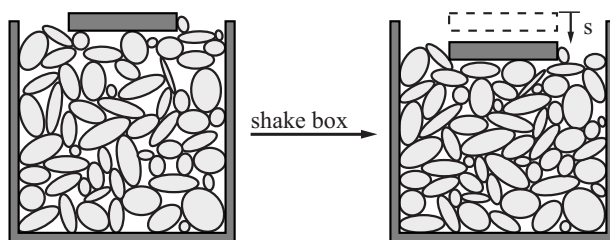


Fig. 3. Densification of a loose granular assembly due to shaking in a box. A foundation on top of the sample eventually will move downwards.

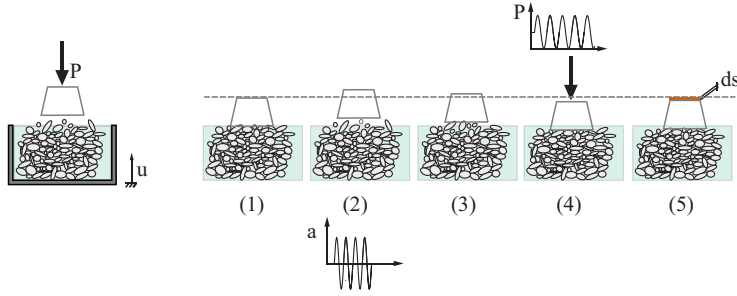


Fig. 4. Exemplary representation of the load history and deformations in a local ballast cell. Vibrations and repeated cyclic load sequences lead to permanent changes in the ballast structure. In general, small increments of settlement accumulate to a track degradation over time.

sequence of mechanisms. In reality, an alternating sequence of various loadings will occur.

(2) **Global picture:** Compaction or loosening in the vibrating box describes a material phenomenon. However, this observation must be embedded in a loading scenario for the entire track–bridge interaction. The complex situation at the bridge is illustrated in Fig. 5.

The passage of a train leads to repeated loading of the ballast bed over the sleepers. The crossing can cause the bridge superstructure to vibrate. The situation of the ballast superstructure can be simulated locally on a vibrating table. The interaction of the forces acting via the sleepers and the vibrations of the bridge girder is complex. The load position and load distribution across the track are constantly changing. In addition, the sleepers rest unevenly on the ballast bed. The localized deformations under a sleeper are coupled via the ballast bed while the sleepers are fixed with the rail. This complex situation makes it difficult to quantify the permanent vertical track changes.

The lateral stability of the track is of particular interest for the ULS analysis of the train–bridge interaction. Compression forces in the rail may add lateral forces to the sleeper load. The track grid can shift laterally, the track position errors can increase, the lateral track resistance is reduced, and finally, the lateral stability can be lost. This comprehensive picture is the background for testing at the authors' institute.

### 2.3. A discussion on shake table tests with complex loading

Extensive shake table tests on ballasted track have been done for the ERRI D214 report<sup>2</sup> and subsequent research projects.<sup>23,24</sup> Tests have been done in a range of 5–60 Hz with a rail grid of four sleepers or smaller boxes with one sleeper or a part of it. All tests show an amplification of harmonic shake table vibrations to the

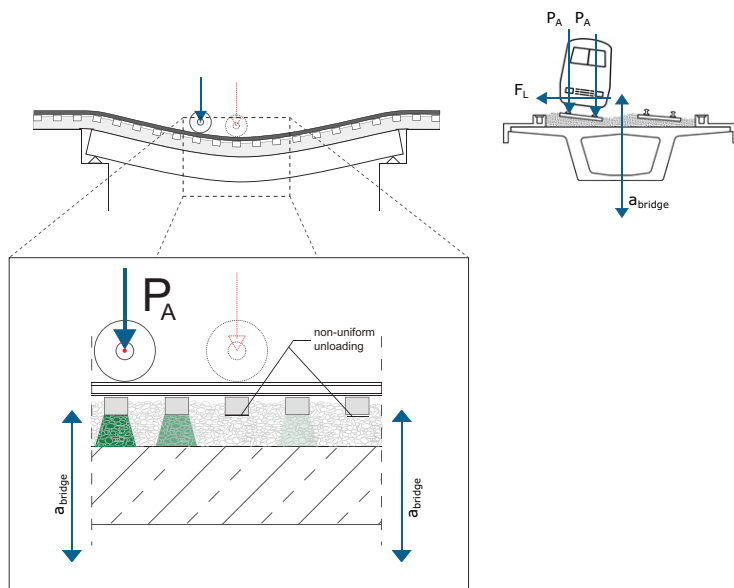


Fig. 5. Track loading scenarios: For the continuation of a track on bridge, the vehicle passing causes bridge deck deflection. A significant vibration of the bridge superstructure might add up (top left). The local track behavior can be investigated on a small section similar to a shake table (bottom left). In addition to the vertical excitation, a lateral loading of the track is of major importance (top right).

upper ballast layer and the sleeper. While vibrations up to 20 Hz do not significantly amplify the amplitude in the track, the trend for higher frequencies is unequivocal (see Fig. 6). Phenomenologically, it is roughly true that at accelerations close to a threshold of 1.0g, ballast particles start to separate and the sleeper bounces on the track bed. At higher frequencies, the amplitudes at the track surface and at the sleepers can be significantly higher than at the vibrating table.

The amplification of amplitudes from the shake table to the ballast is seen as the main reason that the ballast destabilizes also at frequencies >30 Hz. However, for a further understanding of the meaning of such destabilization, it needs to be considered how the performance of the ballast is affected. The following technical considerations must be distinguished<sup>25</sup>:

- Vertical load transfer: The ballast bed must transfer the vertical loads. Tests show that a briefly loosened ballast has the same stiffness after a few cycles of reloading. The utilization of the ballast superstructure is far beyond a state of failure.
- Settlement: Increased settlements do occur. Initially, this is a maintenance problem. Cannot usually be predicted well and — as experience on existing lines shows — may be manageable during operation.



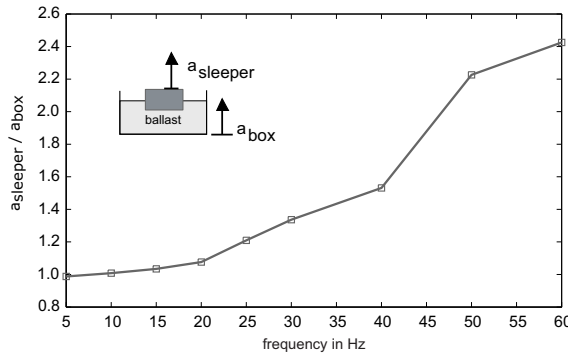


Fig. 6. Exemplified transfer function of shake box accelerations to the sleeper for an acceleration level of 0.7 g. More details on the tests can be found in the literature.<sup>24</sup> Similar behavior was observed for test configurations with a rail grid of four sleepers.

- **Lateral support:** Lateral support is important for keeping the track and preventing loss of lateral stability. The lateral track resistance must not be allowed to drop significantly, nor must lateral track misalignments be allowed to grow uncontrollably.

Subsequently, lateral resistance of the ballast bed has been found most interesting. Track safety can be affected by diminished resistance. Tests were done<sup>12,25</sup> to show how a sleeper's resistance and deformations are affected by the simultaneous effect of a lateral force and an excitation via the vibrating shake table. Figure 7 (left) shows the accumulated lateral displacements of these tests for different acceleration levels and lateral preloads. The test setup included a single B70 sleeper.<sup>12</sup> The excitation frequencies were between 8 Hz and 12 Hz. Previous investigations found the frequencies to not bear relevance.<sup>23</sup>

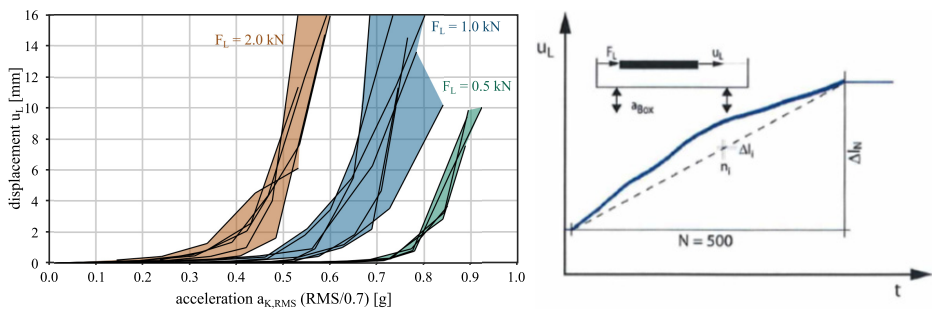


Fig. 7. (left) Accumulation of lateral sleeper displacements for fixed values of lateral load plotted over acceleration amplitude (stepwise increasing). Sequences of 500 vibration cycles. The shaded areas represent maximum and minimum envelopes from different runs of the same test.<sup>12,25</sup> Several tests summarized. (right) Exemplified result for one sequence of 500 vibration cycles.

The accumulation of lateral ballast displacements due to vertical vibrations depends on the amplitude of lateral load and the vertical acceleration amplitude. With some scatter in the data, the lateral displacements for fixed loading parameters increase with nearly constant increments.<sup>12,25</sup> This allows us to formulate a law, expressing the vibration-induced creep  $\Delta f$  as a function of the lateral load  $F_L$  applied on the sleeper, the maximum amplitude  $\hat{a}$  of the vertical accelerations, and the number  $N_{\text{cycl}}$  of cycles. Normalizing the lateral force  $F_L$  by  $F_{L0} = 1 \text{ kN}$  and the acceleration amplitude  $\hat{a}$  by  $a_0 = 1 \text{ g}$  yields the vibration-induced creep in [mm]:

$$\Delta f = \text{sign} \left( \frac{F_L}{F_{L0}} \right) \cdot C_1 \cdot \left| \frac{F_L}{F_{L0}} \right|^{C_2} \cdot \exp \left( C_3 \cdot \frac{\hat{a}}{a_0} \right) \cdot N_{\text{cycl}}. \quad (1)$$

There are no final conclusions about the range of probable values for the constants  $C_1$ ,  $C_2$ , and  $C_3$ . For a specific test setup,<sup>12,25</sup> these values provided the best fit for the experimental data:

$$\begin{aligned} C_1 &= 9.0 \times 10^{-7}, \\ C_2 &= 3.65, \\ C_3 &= 12.523. \end{aligned} \quad (2)$$

#### 2.4. Summary of the current knowledge on ballast destabilization on bridges

The main points of the preceding review can be summarized as follows:

- Ballast destabilizes for base acceleration amplitudes above 0.7 g. Destabilization is a vague labeling for a process of ballast particle reorganization, associated with a loss of strength and increased deformations.
- Generally, settlements increase with increasing accelerations. The displacements become significant for amplitudes of 0.7–0.8 g. However, the vertical stiffness is regained after reloading. The load-bearing capacity is not affected.
- Lateral displacements of a sleeper are strongly dependent on the acceleration amplitude (if accompanied by lateral forces).
- From a local perspective, higher frequencies up to 60 Hz are not less critical than lower frequencies. Of course, higher frequencies are usually associated with smaller wavelengths, thereby limiting the destabilization to local spots.
- So far, an excitation with only single peaks of higher amplitudes has not been proven to be less critical than a large sequence of vibration cycles. Even a few single acceleration peaks disturb the ballast fabric leading to a loosening and then reconfining of the material. However, this has only been proven for (vertical) settlements, but not for the lateral resistance of a sleeper. The question of the significance of non-resonant individual peaks is of central importance in some studies.<sup>26</sup>

- It has been discussed that the vertical behavior of the track is foremost a maintenance problem. It seems justified that for existing bridges that have slightly higher acceleration amplitudes than 0.35 g but otherwise exhibit a technically inconspicuous behavior, these higher amplitudes are tolerated. Such approaches are being pursued by various railway operators.
- The lateral stability of the track is crucial for the safety assessment of a vibrating bridge deck. The lateral displacements of a sleeper on a vibrating bridge deck can be calculated with an empirical formula. Subsequently, this can be used to verify the lateral stability of the track under compression forces in the rails.

While the basic mechanisms of deterioration of a ballasted track are understood, there is still a need to quantify individual effects more reliably and to bring them into an assessment scheme. Some of the findings are based on a few tests. With respect to lateral stability, tests have only been done as static lateral load tests or for harmonic sequences of vibrations with uniform amplitudes. This indicates a certain behavior, but in a real track all load components vary with the train passage, thermal boundary conditions and initial track quality.

In the *InBridge4EU* project, additional analyses are carried out for this purpose. These investigations focus on the provision of more test data especially on questions like the impact of single peaks on the degradation of a ballasted track. But also dedicated verification scenarios for the assessment of bridge accelerations are presented which in the future should allow for a more reliable verification of railway bridges with ballasted track. Details on both interconnected topics are presented below.

### 3. New Test Setup and First Results

#### 3.1. Setup

The aim of the test setup is to examine the vibration-induced creep under different scenarios and with different parameters. A box with inside dimensions of  $1.40\text{ m} \times 1.04\text{ m} \times 0.60\text{ m}$  is filled with ballast, in which a concrete block of  $0.6\text{ m} \times 0.3\text{ m} \times 0.22\text{ m}$  is placed as a model sleeper. The box is enclosed by a frame that rests on a cylinder rod connected to an actuator below the floor plate. Guides on the sides of the enclosing frame enable the box and its enclosing frame to move vertically while all other movements are restrained. An actuator horizontally mounted on the box is used to apply a lateral load on the model sleeper. Four accelerometers (Metra MMF KD41V) mounted at the base plate of the box are used to measure the vibrations. The horizontal displacement of the model sleeper is measured with two laser-optical distance sensors (Micro-Epsilon optoNCDT 1401) which are directed to L-brackets mounted on the sleeper. For preconditioning the ballast and the model sleeper placed within, a vertical actuator mounted on the enclosing frame can apply

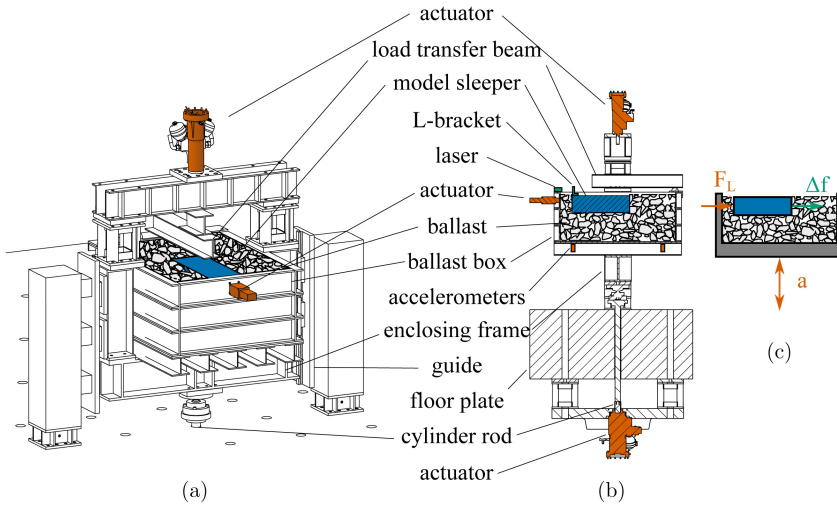


Fig. 8. Experimental setup for examining the vibration-induced creep due to lateral load and vertical vibrations in isometric view (a) and longitudinal section (b). The quantities relevant for the tests are the lateral force  $F_L$ , the box acceleration  $a$ , and the lateral displacement  $\Delta f$ , as shown in (c).

forces on top of the model sleeper. Figures 8(a) and 8(b) show the experimental setup in an isometric view and as a section.

To examine vibration-induced creep, the lateral displacement  $\Delta f$  of the model sleeper is measured while it experiences a lateral force, and the box is subject to vertical vibrations. The governing factors are the lateral force  $F_L$  and the accelerations  $a$  experienced by the ballasted due to the vibrations of the box. Figure 8(c) shows the principle of the tests and the quantities of interest.

There is already a body of knowledge on vibration-induced creep.<sup>12</sup> Two pre-tentional favorable influences that could possibly be neglected in the assessment are frequencies above 30 Hz and single acceleration peaks.<sup>26</sup> The latter one is the subject of this study.

### 3.2. First results

To investigate the effect of single vertical acceleration peaks on vibration-induced lateral creep, comparative experiments are conducted for both harmonic vertical vibrations and impulse loads of single vertical acceleration peaks. Results from the experiments are expected to show significant variation between tests since every test exhibits a slightly different configuration of the ballast in the box.<sup>25</sup> Therefore, to be able to compare harmonic versus impulse accelerations, these two acceleration loading regimes are applied consecutively in a single test. Two tests were conducted, and their results are presented below.

Table 2. Parameters of the tests.

Test	Pre-conditioning	Test procedure	Lateral force
1	Ballast compaction; Sleeper pre-loading 1 000 cycles of 20 kN at 1 Hz	$2 \times 500$ cycles harmonic load, 250 single peak impulses	1.0 kN
2	Ballast compaction; Sleeper pre-loading 1 000 cycles of 20 kN at 1 Hz	250 single peak impulses, $5 \times 500$ cycles harmonic load	1.0 kN

Pre-tests show a lateral resistance of the model sleeper of about 4 kN. To stay well below this limit, a constant lateral force of  $F_L = 1.0$  kN is applied for the tests of vibration-induced creep. The ballast and the model sleeper are pre-conditioned by applying a compaction procedure to the ballast with a vibrating plate and the application of a harmonic load of 20 kN on the sleeper at a frequency of 1 Hz for 1 000 cycles. The aim of this pre-conditioning procedure is to facilitate reproducible conditions.

The first test comprises a harmonic acceleration of  $2 \times 500$  cycles at 30 Hz followed by 250 single peak impulses separated by 3 s. The second test starts with 250 single peak impulses separated by 3 s and follows with  $5 \times 500$  cycles of harmonic acceleration at 30 Hz. Table 2 summarizes the parameters of the tests.

The measured signals of box acceleration and lateral force and displacement are postprocessed with a low-pass filter at 250 Hz. Afterwards, the peaks of the maximum downward acceleration (negative sign) are identified. Figure 9 shows close-up views of the acceleration time series of test 1, including the identified peaks. Figure 10 gives an overview of the results of test 1. The identified acceleration peaks and the measured lateral displacement are plotted over the number of cycles. Likewise, Figs. 11 and 12 show close-up time series and results for test 2, respectively. The results indicate that single acceleration peaks influence the lateral displacement

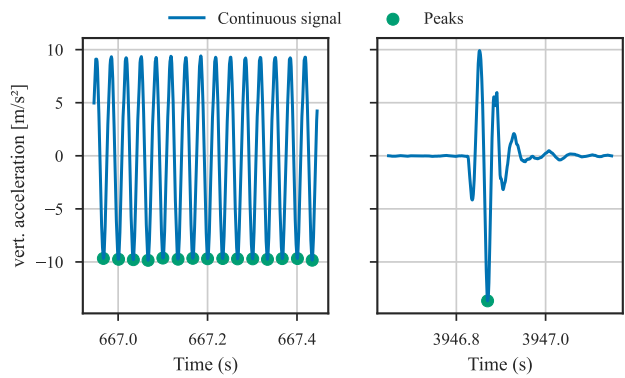


Fig. 9. Close-up view of time series of the measured vertical box accelerations and peaks of the maximum downward acceleration for test 1. The signal on the left is from the harmonic shaking, while the signal on the right is from the transient impulse phase.

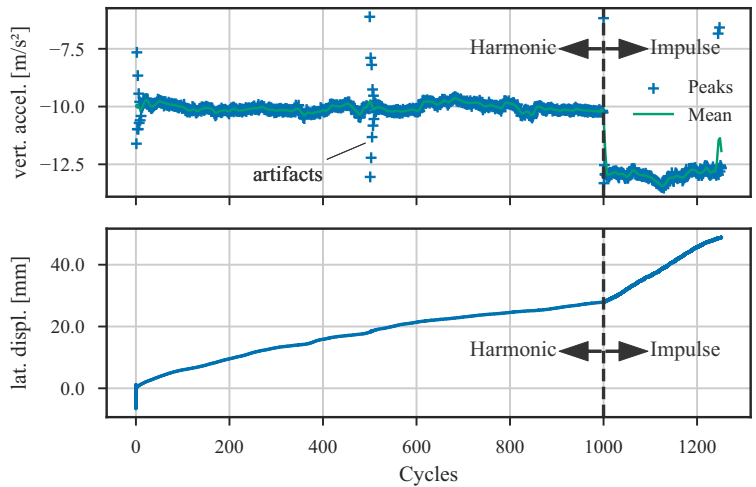


Fig. 10. Aggregated results of test 1. Peaks of the maximum downward vertical box acceleration over the number of cycles (above) and lateral displacement of the model sleeper (below). Artifacts of higher and lower peaks due to the actuator control can be seen at the start of each set of 500 harmonic load cycles.

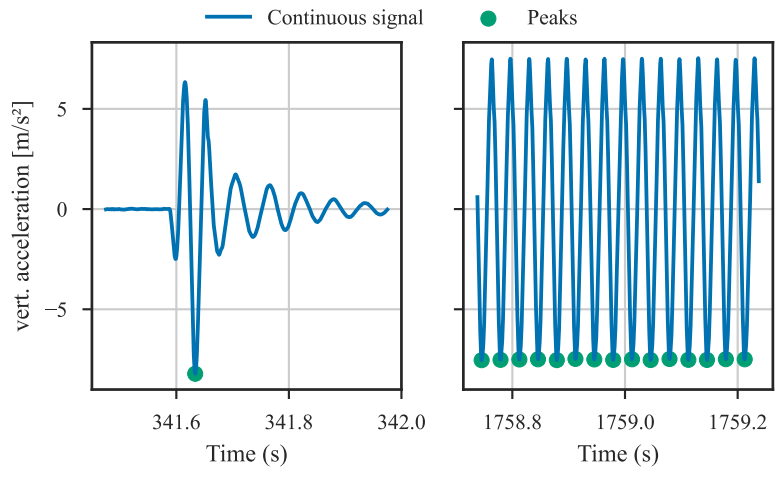


Fig. 11. Close-up view of time series of the measured vertical box accelerations and peaks of the maximum downward acceleration for test 2. The signal on the left is from the transient impulse phase, while the signal on the right is from the harmonic shaking.

of the sleeper on the same scale and single peaks cannot be ignored. Quantifying this effect could be subject to further research.

The assessment must take into account that, in addition to the bridge vibrations, relevant lateral forces must also occur in the track at the same time. High-rail temperatures or lateral vehicle forces are typically not permanently present.

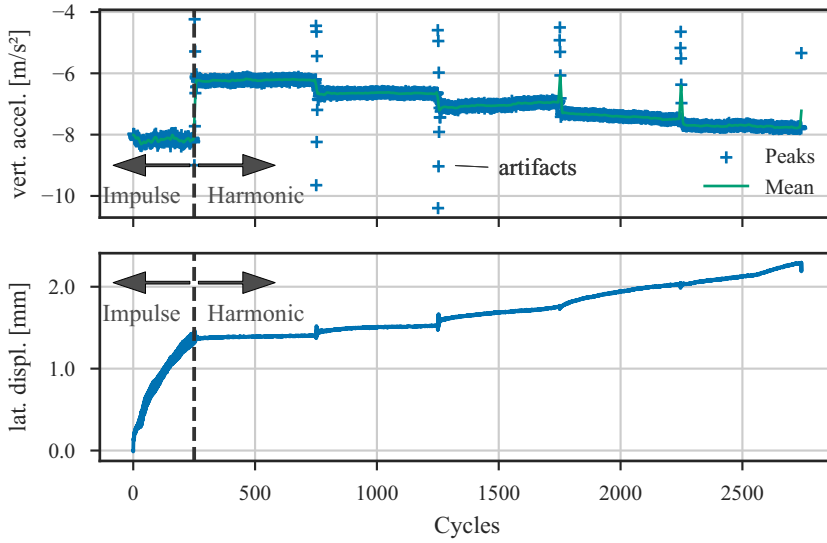


Fig. 12. Aggregated results of test 2. Peaks of the maximum downward vertical box acceleration over the number of cycles (above) and lateral displacement of the model sleeper (below). Artifacts of higher and lower peaks due to the actuator control can be seen at the start of each set of 500 harmonic load cycles.

#### 4. Assessment

The open question remains on how to appropriately describe the limits of ballasted tracks subject to vertical vibrations beyond restricting maximum accelerations to the conservative limit of  $3.5 \text{ m/s}^2$ . Vibration-induced creep leads to lateral displacements of the track. Maintenance regimes are designed to detect and correct flaws in the geometry of the track. Our approach is to cast the question of limits as both a maintenance and geotechnical issue, defining a deflection limit  $\Delta f_{\text{lim}}$  within a given reference timeframe  $t_R$  deriving from geometrical limits of the track given for line categories and maintenance intervals, such as imposed by Ril 821.2001, for example.<sup>27</sup> A lateral track model and a dynamic train-bridge model are employed to estimate the lateral loads on the sleepers and the vertical acceleration the track is subject to. The dynamic analysis yields vertical acceleration time series which are processed further. For different scenarios occurring during the reference timeframe, the lateral creep is evaluated according to Eq. (1). Then, the creep resulting from the different scenarios is superposed and evaluated against the deflection limit. With this approach, one can quantify and evaluate the adverse effects of vibration-induced creep on the track stability due to vibrating bridge decks. This is a deterministic approach that relies on values based on the best fit of a specific test (see Eq. (2)), so special considerations must be taken to account for uncertainty.

#### 4.1. A lateral model

For the calculation of the lateral forces  $F_L$  acting on the sleeper, a lateral track model is formulated as a two-dimensional finite element (FE) model with beam elements representing the track. The necessary parameters are derived from the track geometry, such as the track radius  $r$  and the length  $l$  of the model. Crucial for the lateral forces are the misalignment amplitude  $\delta$  and its length  $l_\delta$ . The sleeper spacing and considerations of the lateral and rotational stiffness<sup>28</sup> influence the modeling of the lateral support of the track. The properties of the beam elements are largely influenced by the rails and can conservatively be assumed as a superposition of two independent rails. Depending on the specified scenarios, a uniform temperature difference  $\Delta T$  is applied to the model. Figure 13 shows the lateral track model and key geometrical parameters. More sophisticated track models can be utilized to examine buckling<sup>28</sup> or describe nonlinear effects of accumulated vibration-induced creep.<sup>12,25</sup> For the current evaluation, with the linear-elastic track model the lateral forces  $F_L$  at the sleepers can be determined.

#### 4.2. A proposal for assessment

The ultimate goal is to assess whether bridge deck vibrations due to high-speed train passages lead to inadmissible lateral track displacements. The track maintenance requirements inform the deflection limit  $\Delta f_{\text{lim}}$  within a given reference timeframe  $t_R$ . Thus, not a single limit state is considered, but likely scenarios occurring within the reference timeframe  $t_R$  are investigated. The displacements  $\Delta f$  of the vibration-induced creep of these scenarios are accumulated and compared with the deflection limit  $\Delta f_{\text{lim}}$ .

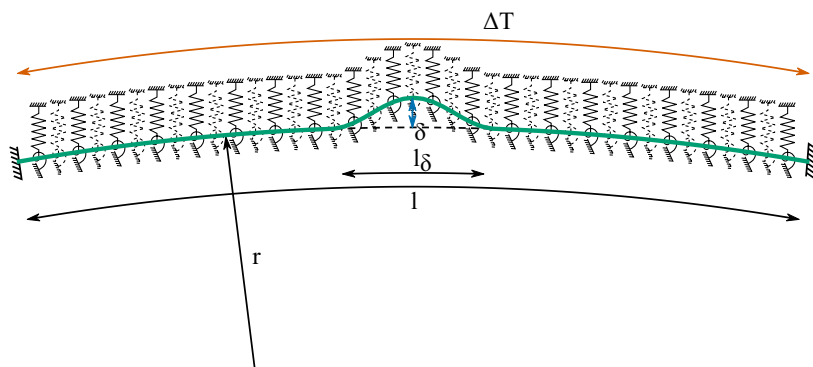


Fig. 13. Lateral model of the track. Key geometrical parameters are the length and radius of the track, the amplitude and length of the imperfection. The scenarios examined prescribe the temperature difference  $\Delta T$  applied to the entire track.



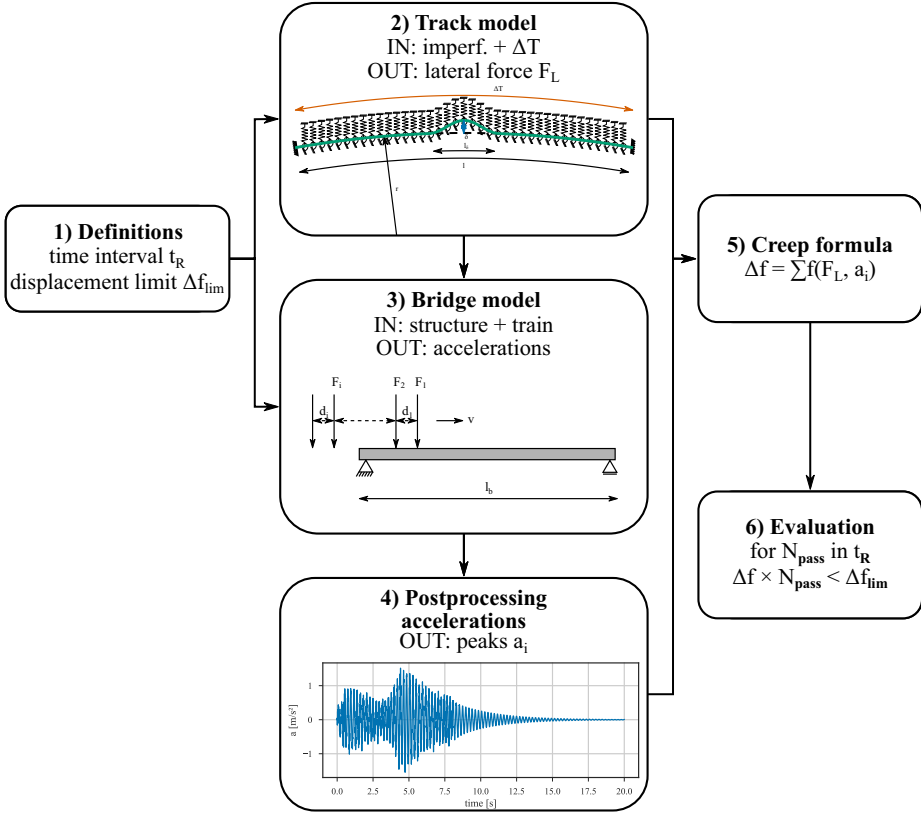


Fig. 14. Workflow for evaluating the lateral displacements due to vibration-induced creep for a given bridge and a given train passage.

The specific workflow of the proposal for assessment is shown in Fig. 14 and comprises the following steps:

- Definition of the limit state:** Define a limit of the lateral deflections  $\Delta f_{lim}$  within a reference timeframe  $t_R$  (e.g. from track inspection regulations such as Ril 821.2001).<sup>27</sup> Define the number of passages in the given reference time interval  $t_R$  as  $N_{pass}$ .
- Track model analysis:** Formulate a model of the track, including imperfections. For a given temperature change  $\Delta T$  of a scenario, calculate the lateral forces  $F_L$  at the sleepers.
- Train-bridge dynamic analysis:** Formulate a model of the bridge dynamics and simulate train passages. For a conservative assumption, this can be a worst-case scenario, e.g. a critical HSLM-A or another high-speed train at a speed that induces a resonant response.

- (iv) **Perform a peak or cycle count** along *all* locations of the track axis or determine critical locations beforehand. These counting algorithms yield either pairs of  $(a_i, n_i)$  of counted cycles for pre-defined classes of acceleration amplitudes or a sequence of acceleration peaks  $a_i$ .
- (v) **Lateral displacements for a single passage:** At each sleeper location: With the lateral load  $F_L$  from the track model's  $F_L$ , and the equivalent acceleration amplitudes  $\hat{a}_i$  and numbers  $n_i$  from the peak or cycle count algorithms, calculate the vibration-induced creep  $\Delta f$  via Eq. (1) for a single train passage.
- (vi) **Evaluation for reference timeframe:** Superpose different scenarios and evaluate:

$$N_{\text{pass}} \times \Delta f \leq \Delta f_{\text{lim}}. \quad (3)$$

The formula for vibration-induced creep of Eq. (1) needs to be applied to acceleration time series of the train passages on the bridge. Since the formula was established with laboratory tests of harmonic excitations with a number  $N_{\text{cycl}}$  of cycles with the same fixed acceleration amplitude  $\hat{a}$ , additional considerations must be made to ensure its suitability for application to accelerations occurring on vibrating bridge decks during train passages. Assuming that the creep displacements originating from cycles of different acceleration amplitudes  $\hat{a}$  can be superposed, the creep formula can be re-written as an accumulation of creep displacements of a series of single cycles with different acceleration amplitudes  $a_i$ :

$$\Delta f = \sum_i \text{sign}(F_L) \cdot C_1 \cdot |F_L|^{C_2} \cdot \exp(C_3 \cdot a_i). \quad (4)$$

With this peak detection or cycle count, algorithms can be applied to obtain the acceleration amplitudes  $a_i$  of the acceleration time series of a vibrating bridge deck. Figure 15 shows a visualization of this principle for a series of cycles with the same acceleration amplitude.

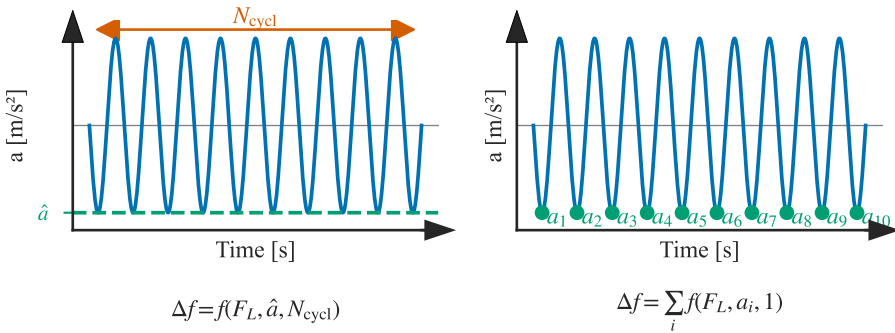


Fig. 15. Visualization of the acceleration input used in the vibration-induced creep formula (left) and the principle of counting the equivalent cycles for the vibration-induced creep formula (right).

### 4.3. Example

To illustrate the proposed method for assessment, the complete workflow is walked through for an example of assessing a bridge for one specific high-speed train, the ICE 4. The bridge's properties with a first natural frequency of  $n_0 = 4.5$  Hz and a span of  $l_b = 19.8$  m necessitate a dynamic analysis after EN 1991-2,<sup>29</sup> clause 6.4.4. The dynamic analysis yields acceleration amplitudes larger than  $3.5 \text{ m/s}^2$ . Applying the proposal for assessment for different scenarios seeks to answer the question of whether the track displacements through vibration-induced creep which are accumulated within a reference timeframe are admissible even with acceleration amplitudes exceeding  $3.5 \text{ m/s}^2$ .

#### 4.3.1. Definition of the limit state

The reference timeframe  $t_R$  is chosen in such a way that a lateral deflection  $\Delta f_{\text{lim}} = 0.5 \text{ mm}$  should not be exceeded. The relevant lateral forces  $F_L$  occur only at large temperature differences  $\Delta T$ . Three scenarios are examined as follows:

- $N_{\text{pass}} = 100$  at  $\Delta T = 40 \text{ K}$ ,
- $N_{\text{pass}} = 100$  at  $\Delta T = 30 \text{ K}$ ,
- and a mixed scenario with  $N_{\text{pass}} = 10$  at  $\Delta T = 40 \text{ K}$ ,  $N_{\text{pass}} = 20$  at  $\Delta T = 30 \text{ K}$ ,  $N_{\text{pass}} = 20$  at  $\Delta T = 20 \text{ K}$ , and  $N_{\text{pass}} = 40$  at  $\Delta T = 10 \text{ K}$ .

#### 4.3.2. Track model analysis

A track model similar to previously studied models<sup>12,25</sup> is specified according to the parameters listed in Table 3. The lateral stiffness  $k_t$  corresponds to a lateral resistance of 9 kN of a sleeper, which is a typical value.<sup>28</sup> The torsional stiffness  $c_t$  is derived from the literature.<sup>28</sup> Two different misalignment amplitudes are studied:  $\delta = 5 \text{ mm}$  and  $\delta = 10 \text{ mm}$ .

Figure 16 shows the model and the resulting lateral forces at the sleepers for both misalignment amplitudes in the scenario of  $\Delta T = 40 \text{ K}$ . These results will later be used in the creep formula.

#### 4.3.3. Train-bridge dynamic analysis

For the dynamic analysis of the bridge, a FE analysis is conducted. Similar to the track model, two-dimensional beam elements are used. The nodal spacing is equal to the sleeper spacing. Assuming that the sleeper locations coincide with both the spring nodes of the lateral track model and the nodes of the bridge model facilitates convenient handling of the results. The signature of the ICE 4 train exhibits a very large value of the dynamic signature at a wavelength of  $\lambda \approx 9.5 \text{ m}$ .<sup>30,31</sup> With the first natural frequency of the bridge of  $n_0 = 4.5 \text{ Hz}$ , the critical speed for this wavelength

Table 3. Parameters of the lateral track model.

Notation	Parameter	Value
$E_t$	Elastic modulus	210 GPa
$l$	Total length of the track	48 m
$r$	Track radius	5 000 m
$l_\delta$	Length of the misalignment	10.0 m
$\delta$	Amplitude of the misalignment	[5 mm, 10 mm]
$\Delta T$	Temperature difference	[10, 20, 30, 40 K]
$I_t$	Moment of inertia ( $2 \times$ UIC60)	$2 \times 513 \text{ cm}^4$
$A_t$	Area ( $2 \times$ UIC60)	$2 \times 76.7 \text{ cm}^2$
$\alpha$	Thermal coefficient	$1.2 \times 10^{-5} \text{ 1/K}$
$D_{N,t}$	Nodal spacing	0.15 m
$D_S$	Spacing of supported nodes (sleepers)	0.6 m
$k_t$	Lateral stiffness of springs	4 500 kN/m
$c_t$	Torsional stiffness of springs	170 kNm/rad

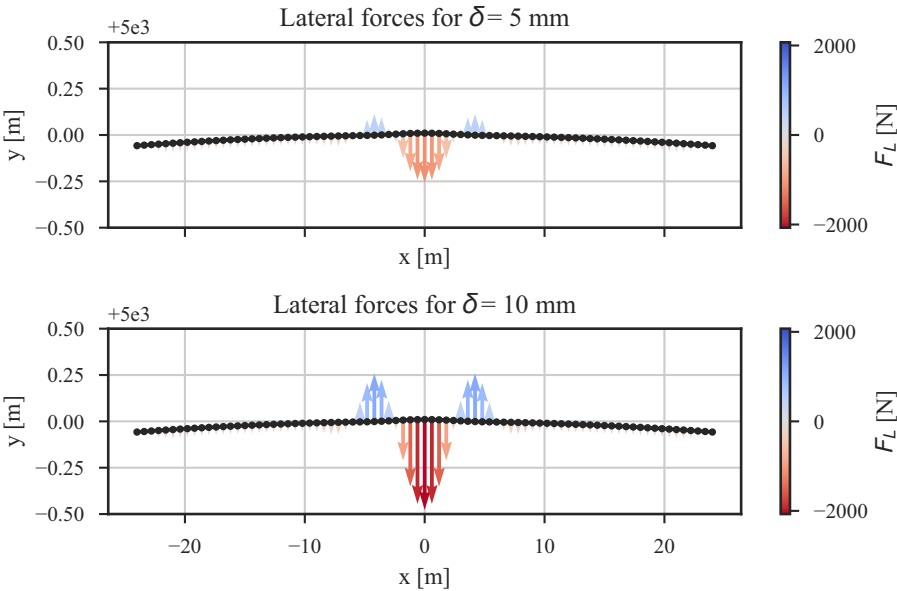


Fig. 16. View of the track model with resulting lateral forces for misalignment amplitudes of 5 mm (above) and 10 mm (below) and a temperature difference of  $\Delta T = 40 \text{ K}$ .

is at  $v = 155 \text{ km/h}$ . The train is modeled as a sequence of moving loads.<sup>32</sup> Table 4 summarizes the parameters of the bridge and the corresponding FE model.

A time-step integration is performed in the modal domain with the Wilson-theta method using a time step of  $\Delta t = 0.2 \text{ ms}$ . The first three bending eigenmodes ( $n_0 = 4.5 \text{ Hz}$ ,  $n_1 = 18.0 \text{ Hz}$ , and  $n_2 = 40.0 \text{ Hz}$ ) are considered. In this example,

Table 4. Parameters of the dynamic train-bridge model.

Notation	Parameter	Value
$E_b$	Elastic modulus	35 GPa
$l_s$	Bridge span	19.8 m
$l_b$	Total bridge length	21.0 m
$I_b$	Second moment of inertia	0.888 m <sup>4</sup>
$A_b$	Area	6.234 m <sup>2</sup>
$\mu$	Distributed mass	24.31 t/m
$D_{N,b}$	Nodal spacing	0.6 m
$\zeta$	Modal damping	0.013
	Train	ICE 4
$v$	Speed	155 km/h
$\Delta t$	Time step for integration	0.2 ms

higher modes are neglected. This choice was deemed sufficient in the current example. Choices regarding the modeling of the dynamics will be different for other examples. A requirement for the proposed assessment procedure is that the numerical models used should have appropriate sophistication to realistically describe the dynamics. The resulting acceleration time series at each node are used in the further analysis.

#### 4.3.4. Perform a peak count

To obtain the necessary information for the creep formula, the peaks of the acceleration time series at each node must be identified. There is no empirical insight into vibration-induced creep at low acceleration amplitudes.<sup>12</sup> Therefore, a threshold of an acceleration of 2 m/s<sup>2</sup> in downward direction (negative sign in our example) is defined, which peaks are required to surpass. The segments of the signals that are below the threshold are identified and their minimum values are counted as peaks. Figure 17 shows the acceleration time series of the midspan node with the identified peaks. Together with the lateral forces  $F_L$ , these peaks now form the basis for calculating the vibration-induced creep.

#### 4.3.5. Lateral displacements for a single passage

The lateral displacements of the track are evaluated for a single train passage. For this, the nodes of the lateral track model and the dynamic train-bridge model need to be matched. In the present example, it is assumed that the maximum misalignment amplitude of the lateral track model coincides with the midspan of the bridge where the highest acceleration amplitudes occur. The accumulation of the creep is calculated according to Eq. (4). In the formula, the values for the constants are assumed to confirm to Eq. (2). Figure 18 shows the results for both misalignment amplitudes and all three scenarios.

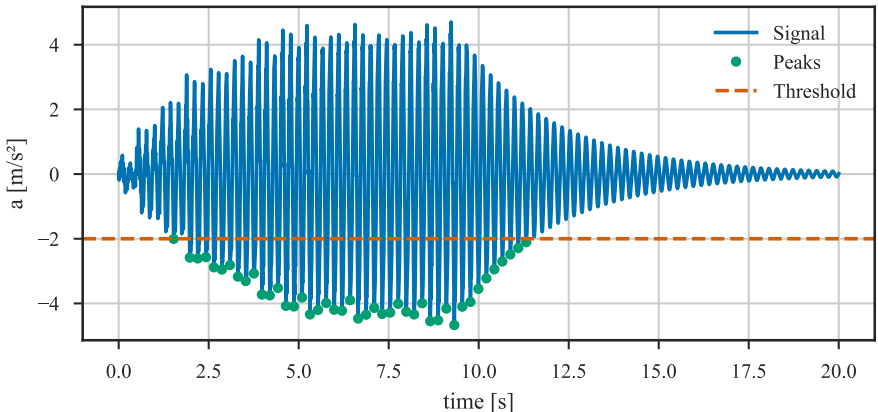


Fig. 17. Time series of the accelerations at the midspan node of the FE model for a passage of an ICE 4 at 155 km/h. The peaks shown are calculated via the peak-counting procedure with a threshold of  $-2.0 \text{ m/s}^2$ .

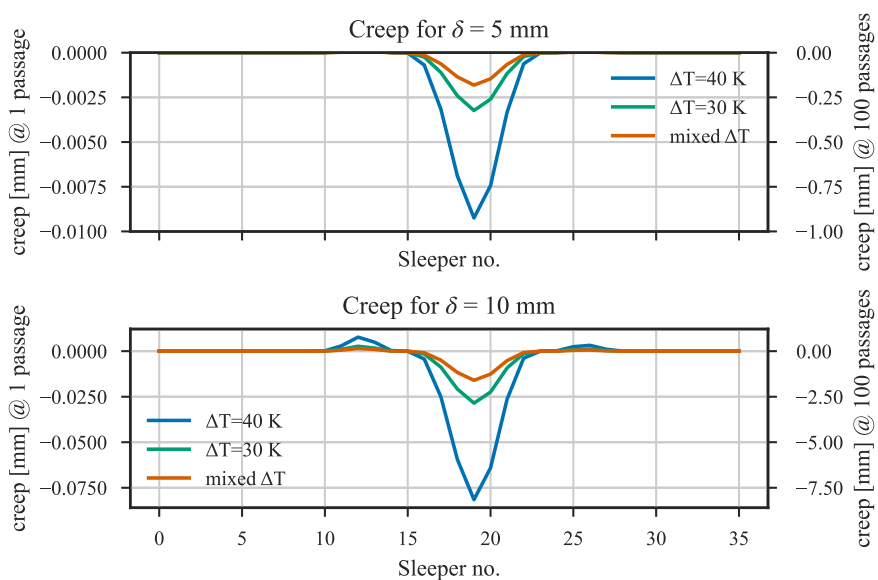


Fig. 18. Vibration-induced creep of the sleepers (which coincide with the nodes of the FE models). The creep is calculated for a single passage of an ICE4 at 155 km/h and for 100 passages.

#### 4.3.6. Evaluation for the reference timeframe

The limit state was defined such that the lateral displacements should not exceed  $\Delta f_{\text{lim}} = 0.5 \text{ mm}$  for a total of  $N_{\text{pass}} = 100$  passages. The results show that this is only given for a misalignment amplitude of  $\delta = 5 \text{ mm}$  for the scenarios of  $\Delta T = 30 \text{ K}$  and a mixed  $\Delta T$ .

## 5. Discussion

With the proposed method for assessing the lateral track stability of ballasted tracks for vibration-induced creep on railway bridges, it is possible to close the gap between railway bridge dynamics and the mechanisms of track destabilization.

However, there are some limitations to the presented approach. Many of these limitations point to future research directions:

- The linear superposition of vibration-induced creep of different acceleration amplitudes, as proposed in Eq. (4) is an assumption. Further examinations, possibly accompanied by experimental tests, would be beneficial in order to know the limits of this assumption.
- There is variability in the results of the peak identification and cycle counting procedures, as they rest on assumptions and parameters such as the threshold value used in the example. In a recent master's thesis<sup>33</sup> a cycle counting algorithm has been investigated. If the results achieved with different parameters and procedures are compared, the uncertainty could be studied further.
- Just a linear-elastic model of the track is used. The load redistribution effects from lateral displacements are neglected. Integrating the lateral track model and the dynamic train-bridge model could address this issue.<sup>12,25</sup>
- In the models employed in the proposed assessment procedure, many parameters are specified (see Tables 3 and 4). Currently, there is no evaluation of their relative importance. A sensitivity study<sup>12</sup> on a similar lateral track model studied the influence of parameters such as temperature, misalignment amplitude, and track radii. A sensitivity analysis like this could be advantageous for the current proposal as well.
- The lateral track model is used to calculate lateral forces due to thermal loads. However, vehicle-induced lateral forces are possible too, due to centrifugal forces, bogie-induced forces due to hunting and nosing, wheel-rail contact forces, and lateral components of vertical forces due to track deficiencies.<sup>34,35</sup> Likewise, vehicles induce vertical forces, which increase the lateral resistance of sleepers.<sup>35</sup> The load case investigated in this study excludes both the beneficial effects of vertical forces and the detrimental lateral forces induced by vehicles on the track.
- The validity of the vibration-induced creep formula, the values of its constants  $C_1$  through  $C_3$ , and its application limits are based on a range of shake table experiments. The variability of the determined constants and the possible limits of the application of the formula can be further studied with experiments. Current research utilizes Discrete Element Models (DEMs) to understand lateral sleeper resistance.<sup>36–38</sup> Carefully calibrated DEMs<sup>39</sup> could help investigate different application scenarios.
- The proposed assessment procedure enables a deterministic assessment of scenarios. A more thorough approach would be to run a probabilistic analysis that

includes uncertainty in the parameters of the three models: (a) the lateral track model, (b) the dynamic train-bridge model, and (c) the creep formula. Analogously, recent work has examined this for ballastless tracks.<sup>8</sup>

The strength of the presented proposal is that it considers both bridge and track for an assessment of the vibration-induced creep. Concrete scenarios of a specific bridge, specific train, and a specific track can be analyzed. With such an analysis, it is possible to assess bridges for high-speed traffic even if the peak acceleration amplitudes are larger than  $3.5 \text{ m/s}^2$  which is currently prescribed by design codes.

## 6. Summary and Concluding Remarks

This paper addresses ballasted tracks on vibrating bridge decks by describing the physical mechanism involved and presents the relevant past and present experimental findings. The ballast bed destabilizes if the vertical oscillation amplitudes approach the order of gravity  $g$ , whereby — with scattering — clear indications are usually already visible at an amplitude of  $\sim 0.7g$ . Even if this is often called into question, it can generally be stated that this also applies to frequencies greater than 30 Hz. Destabilization is a somewhat vague term. In that respect, it is argued that ensuring the lateral support effect of the ballast is considered particularly important.

To investigate existing gaps in knowledge an updated testing setup with a shake box is used. Tests show that even single pulses of the vibrating table in the ballast bed lead qualitatively to the same displacements as resonance-type load sequences. Further investigations are necessary for a more precise quantification.

Ensuring the lateral stability of the track is considered essential for the assessment. The accumulation of lateral ballast displacements due to vertical vibrations, termed vibration-induced creep, is the most significant detrimental effect of vibration bridge decks on ballasted tracks. Different load events such as compression forces in the rails, which originate from temperature increase, and different vibration amplitudes are superimposed. Due to the creep behavior of the sleepers in the ballast bed, it is not possible to simply superimpose the load events. A proposal for the assessment of specific track, bridge, and train combinations is made, enabling it to go beyond the current restrictions of the design and reassessment codes.

In addition to the directions for future research deriving from the limitations of the proposal for assessment, two main future research directions are as follows:

- Extending the knowledge on vibration-induced creep through further experiments and simulations.
- Integrating probabilistic analyses<sup>8,40</sup> of dynamic train-bridge models with probabilistic analyses of lateral track models.



## Acknowledgments

The authors would like to acknowledge the financial support of Europe's Rail Joint Undertaking through the project *InBridge4EU — Enhanced Interfaces and train categories for dynamic compatibility assessment of European railway bridges* (Grant agreement number 101121765), funded by European funds through Horizon Europe. The discussion with the project research colleagues and with the railway track managers is gratefully acknowledged.

## ORCID

Matthias Baeßler  <https://orcid.org/0000-0002-5182-7310>

Patrick Simon  <https://orcid.org/0000-0002-1538-177X>

## References

1. J. M. Goicolea-Ruigómez, Service limit states for railway bridges in new design codes IAPF and eurocodes, in *Track-bridge Interaction on High-speed Railways* (CRC Press, 2008), pp. 17–28.
2. ERRI Committee, ERRI D214/RP9 Rail bridges for speeds >200 km/h, Final report (1999).
3. T. Heiland, M. Hägle, T. Triantafyllidis, L. Stempniewski and A. Stark, Stiffness contributions of ballast in the context of dynamic analysis of short span railway bridges, *Constr. Build. Mater.* **360** (2022) 129536, doi:10.1016/j.conbuildmat.2022.129536.
4. A. Stollwitzer, J. Fink and T. Malik, Experimental analysis of damping mechanisms in ballasted track on single-track railway bridges, *Eng. Struct.* **220** (2020) 110982, doi:10.1016/j.engstruct.2020.110982.
5. T. Rauert, H. Bigelow, B. Hoffmeister and M. Feldmann, On the prediction of the interaction effect caused by continuous ballast on filler beam railway bridges by experimentally supported numerical studies, *Eng. Struct.* **32** (2010) 3981–3988, doi:10.1016/j.engstruct.2010.09.009.
6. J. Chordà-Monsonís, A. Romero, E. Moliner, P. Galvín and M. D. Martínez-Rodrigo, Ballast shear effects on the dynamic response of railway bridges, *Eng. Struct.* **272** (2022) 114957, doi:10.1016/j.engstruct.2022.114957.
7. E. Moliner, M. D. Martínez-Rodrigo and P. Museros, Dynamic performance of existing double track railway bridges at resonance with the increase of the operational line speed, *Eng. Struct.* **132** (2017) 98–109, doi:10.1016/j.engstruct.2016.11.031.
8. G. Ferreira, P. Montenegro, A. Andersson, A. A. Henriques, R. Karoumi and R. Calçada, Critical analysis of the current Eurocode deck acceleration limit for evaluating running safety in ballastless railway bridges, *Eng. Struct.* **312** (2024) 118127, doi:10.1016/j.engstruct.2024.118127.
9. P. Galvín, A. Romero, E. Moliner, G. De Roeck and M. D. Martínez-Rodrigo, On the dynamic characterisation of railway bridges through experimental testing, *Eng. Struct.* **226** (2021) 111261, doi:10.1016/j.engstruct.2020.111261.
10. CEN - European Committee for Standardization, EN 1990:2023-03 Eurocode – Basis of structural and geotechnical design (2023).
11. Austrian Standards International, ÖNORM B 4008-2:2019-11-15 Assessment of load capacity of existing structures — Part 2: Bridge construction (2019).

12. M. Baeßler, P. Cuéllar and W. Rücker, The lateral stability of ballasted tracks on vibrating bridge decks, *Int. J. Railw. Technol.* **3** (2014) 1–22, doi:10.4203/ijrt.3.2.1.
13. T. Nakamura, Y. Momoya, K. Nomura and Y. Yoshihiko, Shaking table test using full-scale model for lateral resistance force of ballasted tracks during earthquake, *Procedia Eng.* **143** (2016) 1100–1107, doi:10.1016/j.proeng.2016.06.156.
14. M. Esmaeili, S. A. S. Hosseini and M. Sharavi, Experimental assessment of dynamic lateral resistance of railway concrete sleeper, *Soil Dyn. Earthq. Eng.* **82** (2016) 40–54, doi:10.1016/j.soildyn.2015.11.011.
15. G. Jing and P. Aela, Review of the lateral resistance of ballasted tracks, *Proc. Inst. Mech. Eng. F: J. Rail Rapid Transit* **234** (2020) 807–820, doi:10.1177/0954409719866355.
16. M. Baeßler, J. Bronsert, P. Cuéllar and W. Rücker, Evaluating the degradation of ballasted track at bridges for high-speed railways, in *Proc. IABMAS 2014 — 7th Int. Conf. Bridge Maintenance, Safety and Management*, eds. A. Chen, D. M. Frangopol and X. Ruan (CRC Press, Shanghai, China, 2014), pp. 1–8.
17. InBridge4EU, Enhancing European railway bridge standards (n.d.), <https://inbridge4eu.eu/> (Accessed 29 January 2025).
18. P. Vielsack, Pseudo viscosity and dry friction, *Geotechnik* **13** (1991) 11–15 (in German).
19. M. J. Shenton, Deformation of railway ballast under repeated loading conditions, in *Railroad Track Mechanics and Technology* (Elsevier, 1978), pp. 405–425, doi:10.1016/B978-0-08-021923-3.50025-5.
20. P. N. Gaskin, A. G. Powell and G. Raymond, Response of railroad ballast to vertical vibration, *Transp. Eng. J. ASCE* **104** (1978) 75–87, doi:10.1061/TPEJAN.0000694.
21. J. G. D. Morgan and E. Markland, The effect of vibrations on ballast beds, *Géotechnique* **31** (1981) 367–386.
22. T. Mogami and K. Kubo, The behaviour of soil during vibration, in *Proc. 3rd Int. Conf. Soil Mechanics and Foundation Engineering* (Zürich, Switzerland, 1953), pp. 152–155.
23. M. Zacher and M. Baeßler, Dynamic behaviour of ballast on railway bridges, in *Dynamics of High-speed Railway Bridges* (CRC Press, 2008), pp. 125–142.
24. W. Rücker, M. Baeßler and R. G. Rohrmann, Experimental investigations of ballasted tracks on bridges, in *Entwicklungen in der Bodenmechanik, Bodendynamik und Geotechnik*, ed. F. Rackwitz (Springer-Verlag, Berlin, Heidelberg, 2006), pp. 397–414, doi:10.1007/3-540-27438-3\_26 (in German).
25. M. Baeßler, Settlement and stability of ballasted track due to cyclic and dynamic loading, PhD thesis, Technische Universität Berlin (2008), doi:10.14279/depositonce-1910 (in German).
26. P. Norris, Recent advances in the understanding of bridge dynamic behaviour on the West Coast main line route modernisation project, in *Dynamics of High-speed Railway Bridges* (CRC Press, 2008) pp. 157–180.
27. DB Netz AG, Richtlinie 821.2001 Prüfung der gleisgeometrie mit gleismessfahrzeugen (2020).
28. M. A. Van, Stability of continuous welded rail track, PhD thesis, TU Delft (1997).
29. DIN Deutsches Institut für Normung e. V. (German Institute for Standardization), DIN EN 1991-2: 2003 + AC: 2010 Eurocode 1: Actions on structures – Part 2: Traffic loads on bridges – German version (2010).

30. G. Grunert, Data and evaluation model for the description of the static–dynamic interface between trains and railway bridges, *Eng. Struct.* **262** (2022) 114335, doi:10.1016/j.engstruct.2022.114335.
31. A. Kohl, A. Firus, M. Rupp, J. Schneider, M. Kwapisz, A. Vorwagner, M. Reiterer, M. Vospernig, R. Tukhbatullin and G. Lombaert, Bridge Dynamics; Dynamic load model, Deutsches Zentrum für Schienenverkehrsforschung beim Eisenbahn-Bundesamt (2024), doi:10.48755/DZSF.240009.01 (in German).
32. J. M. Goicolea and P. Antolin, The dynamics of high-speed railway bridges: A review of design issues and new research for lateral dynamics, *Int. J. Railw. Technol.* **1** (2012) 27–55, doi:10.4203/ijrt.1.1.2.
33. J. M. Menezes, Modelling of the dynamic behaviour of ballast on railway bridges, Master thesis, Universidade do Porto (2024).
34. J. A. Musazay, A. M. Zarembski and J. W. Palese, Determining track-induced lateral thermal expansion forces on a curved railway track, *Proc. Inst. Mech. Eng. F: J. Rail Rapid Transit* **236** (2022) 3–14, doi:10.1177/0954409721995318.
35. A. Kish, G. Samavedam and D. Wormley, Fundamentals of track lateral shift for high-speed rail applications (1998).
36. C. Shi, A. Andersson, L. Xu and J. Guo, DEM analysis of lateral sleeper resistance: Effect of sleeper-ballast interaction and aggregate friction, in *Proc. Sixth Int. Conf. Railway Technology: Research, Development and Maintenance* (Civil-Comp Press, 2024), pp. 1–14, doi:10.4203/cc.7.24.4.
37. F. Khatibi, M. Esmaili and S. Mohammadzadeh, DEM analysis of railway track lateral resistance, *Soils Found.* **57** (2017) 587–602, doi:10.1016/j.sandf.2017.04.001.
38. Y. Guo, W. Jia, V. Markine and G. Jing, Rheology study of ballast-sleeper interaction with particle image Velocimetry (PIV) and discrete element modelling (DEM), *Constr. Build. Mater.* **282** (2021) 122710, doi:10.1016/j.conbuildmat.2021.122710.
39. Y. Guo, C. Zhao, V. Markine, G. Jing and W. Zhai, Calibration for discrete element modelling of railway ballast: A review, *Transp. Geotech.* **23** (2020) 100341, doi:10.1016/j.trgeo.2020.100341.
40. P. Salcher and C. Adam, Estimating exceedance probabilities of railway bridge vibrations in the presence of random rail irregularities, *Int. J. Struct. Stab. Dyn.* **20** (2020) 2041005, doi:10.1142/S0219455420410059.